Spin-orbit effects in the heavy alkaline-earth atoms

Chris H. Greene
Department of Physics and Joint Institute for Laboratory Astrophysics, University of Colorado, Boulder, Colorado 80309-0440

Mireille Aymar
Laboratoire Aimé Cotton, Centre National de la Recherche Scientifique II, Bâtiment 505, 91405 Orsay CEDEX, France
(Received 28 November 1990)

Complex bound and autoionizing spectra of strontium, barium, and radium are treated at two different levels of approximation using multichannel-quantum-defect techniques (MQDT) and eigenchannel R-matrix calculations. In the first level, the R-matrix calculations are conducted entirely in LS coupling without explicitly including any spin-orbit terms in the Hamiltonian. A subsequent frame transformation to jj coupling is then carried out prior to the MQDT treatment. In the second level, the entire R-matrix calculation is conducted in jj coupling, including spin-orbit terms in the Hamiltonian explicitly within the R-matrix box. The two methods give nearly identical results even for atoms as heavy as barium, each showing good agreement with experiment, but significant differences begin to appear between the two levels of approximation for atomic radium.

I. INTRODUCTION

Recent years have seen a major enhancement in our ability to calculate energy levels, oscillator strengths, and autoionization observables for the alkaline-earth atoms. The combination of an eigenchannel R-matrix approach [1,2] with multichannel-quantum-defect theory [3–5] (MQDT) has now been shown in numerous calculations to describe experimental spectra to spectroscopic accuracy, even for atoms as heavy as strontium [6–8]. Some other progress has been achieved [9] without making use of the power of MQDT, but such methods have only limited applicability to the highly perturbed and overlapping Rydberg series which are the rule in all of these atoms.

In the studies performed to date [6–8], a variational R-matrix calculation is carried out in LS coupling neglecting all fine-structure effects. The interactions between all open and closed channels are then characterized by elements of a smooth reaction matrix K^{LS} and by corresponding dipole matrix elements d^{LS}. This LS-coupled information is then transformed into jj coupling using the well-known orthogonal transformation matrix [10] $\langle jj|LS\rangle$. The spin-orbit terms in the Hamiltonian are now used indirectly, in that the *experimental* j-dependent ionization threshold energies E_i are used when solving the MQDT equations for the continuum states on a finite-energy mesh, just as in earlier semiempirical studies [4,11,12]. This guarantees that Rydberg series will be present converging to each allowed ionization threshold, thus permitting a highly accurate description of spin-orbit effects in light atoms, even when those effects are strongly nonperturbative. In more physical terms, this scheme amounts in effect to neglecting the spin-orbit interaction, except to the extent that energy conservation affects the energy of the outermost electron at $r \geq r_0$.

The high accuracy of calculations based on the above scheme is now well established for Mg [13], for Ca [7], and for Sr [6]. However, in very heavy atoms such as Ba and Ra, this approach is more questionable since spin-orbit effects become much larger and are expected to affect the motion of the outer two valence electrons even at small radii $r \leq r_0$. In the first test of the jj-LS frame transformation in an atom as heavy as Ba, however, Aymar [14] recently showed it to give surprisingly good results, demonstrating largely the same good level of agreement with experiment as had been found previously for Sr [6(a)].

The present study examines in more detail the range of validity of the jj-LS frame transformation by calculating numerous spectra for Sr, Ba, and Ra and comparing the jj-LS calculation with a full jj-coupled calculation that includes spin-orbit terms explicitly in the Hamiltonian even within the R-matrix box. The latter calculations are carried out along the same lines developed in a recent treatment [15] of the alkali-metal negative ions Rb^-, Cs^-, and Fr^-. This fully jj-coupled approach is expected to give a much more realistic description of spin-orbit effects when they are important, and accordingly the comparison of the two types of calculation will help to clarify the range of validity of frame transformation calculations in general. This matter has some practical importance, since each jj-coupled calculation requires 5–10 times more computer time and memory than does an equivalent R-matrix calculation in LS coupling. (This is because for a given total angular momentum J there are typically three times as many jj-coupled channels as LS channels, which translates into roughly nine times as many matrix elements to reach an equivalent level of convergence in jj coupling.) For atoms with only two valence electrons, either approach is modest enough to be performed on a small computer workstation, but an order of magnitude could make an enormous difference in the

feasibility of such calculations for open-shell atoms with more valence-shell electrons.

Accounting for detailed spectroscopy of these heavy atoms, much of it only recently acquired [16], is a second major goal of this paper. Theoretical results are shown to adequately describe photoionization spectra of ground-state strontium and also of the ground state and an excited state of barium. Less experimental information is available for comparison in the case of atomic radium [17–19], but most of the $J=1$, odd-parity bound spectrum which has been observed is in reasonable agreement with the calculations reported here. A single major discrepancy in the radium bound spectrum suggests either a gross misclassification in the early measurements of Rasmussen [17], or else it indicates a serious limitation of the present approach for the heaviest atoms in the Periodic Table. Deciding between these two alternative interpretations may require another experimental measurement of the radium spectrum.

Beyond the issues of agreement or disagreement between theory and experiment are several substantial questions concerning the methods of calculation needed to treat heavy atoms in the Periodic Table. One major question is whether the Schrödinger equation suffices to describe electronic wave functions even in atoms as heavy as radium. The answer expected from traditional multiconfiguration Hartree-Fock-style calculations (MCHF) would be negative, as the inner shell electrons are highly relativistic in radium. However, our present results apparently confirm those of Ref. [15] in suggesting that use of empirical information about the "one-valence-electron" system (e.g., Ra^+) allows one to bypass a full description based on the Dirac equation and to continue using the more convenient Schrödinger description. This and other related issues are addressed below in Sec. IV.

Section II outlines the *jj*-coupled R-matrix approach including spin-orbit effects within the reaction zone. Once the *jj*-coupled reaction matrix and dipole matrix elements have been obtained, the generation of the full spectrum follows standard MQDT formulations. On the other hand, the *LS*-coupled R-matrix calculations are not discussed at depth here since they have been presented in detail elsewhere [6–8,14]. Section III is instead devoted to analyzing the theoretical and experimental spectra of these heavy atoms, with their implications considered further in Sec. IV.

II. EIGENCHANNEL R-MATRIX CALCULATION IN *jj*-COUPLING

The model Hamiltonian used to describe the two valence electrons will be represented as

$$H=T_1+T_2+V(r_1)+V(r_2)+V_{\text{s.o.}}(1)+V_{\text{s.o.}}(2)+\frac{1}{r_{12}} . \tag{1}$$

Here T_1 and T_2 are the usual Schrödinger kinetic-energy operators for each electron. The screening of the nuclear charge Z by the core electrons produces in the end a net electron-core effective potential represented by $V(r_i)$ for the ith electron. The potential $V(r)$ is chosen to have the following analytical form:

$$V(r)=-\frac{1}{r}[2+(Z-2)\exp(-\alpha_1^l r)+\alpha_2^l r\exp(-\alpha_3^l r)] -\frac{\alpha_d}{2r^4}\{1-\exp[-(r/r_c^l)^6]\} , \tag{2}$$

where Z is the nuclear charge and α_d the dipole polarizability of the doubly charged positive ion [14,15]. The empirical parameters α_i^l and r_c^l are adjusted to obtain optimum agreement between the energy eigenvalues E_{nlj} of the one-electron Schrödinger equation and the experimental energies of the alkaline-earth ion. The values of the parameters obtained for Sr^+, Ba^+, and Ra^+ are given in Table I. It is important to note that the potential $V(r)$ depends on the orbital angular-momentum quantum number l of the electron, which makes it formally a nonlocal potential but in a trivial way.

The spin-orbit interaction, e.g., between electron i and the screened nucleus, is represented by a potential having the form

$$V_{\text{s.o.}}(i)=\frac{\mathbf{s}_i\cdot\mathbf{l}_i}{2c^2}\frac{1}{r_i}\frac{\partial V}{\partial r_i}\left[1-\frac{V(r_i)}{2c^2}\right]^{-2} , \tag{3}$$

with $c=137.036$ the speed of light in atomic units. The last factor in Eq. (3) is suggested by the Dirac equation [20], but is typically omitted in perturbation treatments. Here it is included as in some previous studies in order to make solutions to the radial Schrödinger equation well defined near the origin $r_i\to 0$.

The first aim of the calculation is to determine the channel-mixing parameters of multichannel-quantum-defect theory, after which any desired observable can be rapidly calculated. These parameters are determined by solving the Schrödinger equation variationally within the finite reaction volume $\mathcal{V}$ in configuration space, defined by $\max(r_1,r_2)\le r_0$, while the reaction surface $\mathcal{S}$ is the set of all points for which $\max(r_1,r_2)=r_0$. This calculation is also referred to as an *eigenchannel* R-matrix calculation since it determines variationally the *eigenstates* of the R-matrix at some specified energy E, having a constant normal logarithmic derivative on the reaction surface $\mathcal{S}$.

The specifics of the general eigenchannel formulation are derived elsewhere (see, e.g., Ref. [8]), so we only summarize the formulas and the logic followed in their solution. The βth desired eigenstate of the Hamiltonian (and of the R matrix) is represented within $\mathcal{V}$ by a basis-set expansion,

$$|\Psi_\beta\rangle=\sum_k |y_k\rangle Z_{k\beta} , \tag{4}$$

in terms of constant coefficients $Z_{k\beta}$ and a two-electron *jj*-coupled basis set $|y_k\rangle$. The negative of the normal logarithmic derivative of $|\Psi_\beta\rangle$ on $\mathcal{S}$, denoted b_β, constant over $\mathcal{S}$, is determined as an eigenvalue of a generalized eigenvalue problem,

TABLE I. Semiempirical parameters in Eq. (2) describing the model potential experienced by the outermost (valence) electron in Sr^+, Ba^+, and Ra^+.

	l	α_1	α_2	α_3	r_c
Sr^+	0	3.4187	4.7332	1.5915	1.7965
$\alpha_d=7.5$	1	3.3235	2.2539	1.5712	1.3960
	2	3.2533	3.2330	1.5996	1.6820
	≥ 3	5.3540	7.9517	5.6624	1.0057
Ba^+	0	3.0751	2.6107	1.2026	2.6004
$\alpha_d=11.4$	1	3.2304	2.9561	1.1923	2.0497
	2	3.2961	3.0248	1.2943	1.8946
	≥ 3	3.6237	6.7416	2.0379	1.0473
Ra^+	0	3.7702	4.9928	1.5179	1.3691
$\alpha_d=18$	1	3.9430	5.0552	3.6770	1.0924
	2	3.7008	4.7748	1.4956	2.2784
	≥ 3	3.8125	5.0332	2.1016	1.2707

$$\underline{\Gamma}\mathbf{Z}=b\underline{\Lambda}\mathbf{Z} \ . \tag{5}$$

The matrices $\underline{\Gamma}$ and $\underline{\Lambda}$ are defined in terms of the Hamiltonian H in Eq. (1) and the matrix elements of the Bloch operator

$$L_{kk'}\equiv\tfrac{1}{2}\left\langle\!\!\left\langle y_k \left| \frac{\partial}{\partial n} \right| y_{k'} \right\rangle\!\!\right\rangle \ . \tag{6}$$

Here the double bracket matrix element $\langle\langle \ | \ | \ \rangle\rangle$ indicates an integral over the reaction surface $\mathcal{S}$, including a trace over the spin degrees of freedom of the electrons, while single brackets indicate a matrix element over the whole reaction volume. Then Eq. (5) contains a reaction volume overlap matrix element $O_{kk'}\equiv\langle y_k|y_{k'}\rangle$ in addition to the Hamiltonian and Bloch operator matrices,

$$\Gamma_{kk'}=2EO_{kk'}-2H_{kk'}-2L_{kk'} \ . \tag{7}$$

Equation (5) also contains a surface overlap matrix element

$$\Lambda_{kk'}=\langle\langle y_k|y_{k'}\rangle\rangle \ . \tag{8}$$

The basis set used here consists of nonorthogonal jj-coupled independent-electron numerical basis functions, eigenfunctions of the independent-electron Hamiltonian operator $H_0=H-1/r_{12}$. Note that in this basis, both H and H_0 are not Hermitian, but owing to the Bloch operator, Γ is Hermitian.

A. Design of the basis set

The two-electron basis set is composed of one-electron eigenfunctions, obeying

$$(T+V+V_{\text{s.o.}})|n(sl)jm\rangle=E_{nlj}|n(sl)jm\rangle \ , \tag{9}$$

with l and j denoting the one-electron orbital and total angular momenta, and n denoting a "principal quantum number" labeling different radial solutions having the same l and j. An unsymmetrized two-electron eigenfunction jj coupled to form a state of definite total angular momentum J will then be written in notation analogous to that of Biedenharn and Louck [21]

$$|n_1(sl_1)j_1,n_2(sl_2)j_2JM\rangle \ . \tag{10}$$

A fully antisymmetric two-electron basis function is labeled by additional curly brackets $\{\ \}$,

$$|\{n_1(sl_1)j_1,n_2(sl_2)j_2JM\}\rangle=\frac{1}{\sqrt{2(1+\delta_{n_1n_2}\delta_{l_1l_2}\delta_{j_1j_2})}}[\,|n_1(sl_1)j_1,n_2(sl_2)j_2JM\rangle -(-1)^{j_1+j_2-J}|n_2(sl_2)j_2,n_1(sl_1)j_1JM\rangle\,] \ . \tag{11}$$

Thus the basis-vector label k in Eq. (4) is meant as a short-hand notation for the quantum numbers $\{n_1l_1j_1n_2l_2j_2\}$.

In a basis consisting of such jj-coupled two-electron functions it is more or less straightforward to calculate all matrix elements in the variational expression (5) and to determine corresponding eigenvalues $-b_\beta$ of the R matrix. In practice it has proven convenient to specify the two-electron basis in a manner which guarantees that the number of such eigenvalues obtained at any given energy E coincides with the number of channels in the calculation. This can be accomplished using the terminology of "closed-type" and "open-type" two-electron basis vectors, $|y_k^c\rangle$ and $|y_k^o\rangle$, respectively, along the same lines discussed previously for the LS-coupled calculations [6–8,14]. To begin with, two different sets of *one-electron*

orbitals are first defined which obey Eq. (9). The first set is composed of orbitals $|n(sl)j\rangle$ denoted closed-type because they are chosen to vanish at $r=r_0$. Because the closed-type one-electron orbitals each obey the same boundary condition at the origin and at r_0, and because they are eigenfunctions of a Hermitian operator, they are automatically orthogonal over the radial interval $0\le r\le r_0$. The second set of one-electron orbitals is denoted open-type because they will be included in the two-electron basis set only in channels to be treated as open (or weakly closed in the sense of MQDT), and will have the radial quantum number denoted by a bar, i.e, $|\bar{n}(sl)j\rangle$. Then each two-electron closed-type basis vector $|y_k^c\rangle$ is given by Eq. (11), and it consists of two closed-type radial orbitals.

Accordingly, $|y_k^c\rangle$ vanishes on the two-electron reaction surface $\mathcal{S}$. The open-type two-electron basis vector $|y_k^o\rangle$ is instead comprised of a closed-type orbital for n_1, but an open-type one-electron orbital $|\bar{n}_2(sl_2)j_2\rangle$ is used in place of the closed-type $|n_2(sl_2)j_2\rangle$ in Eq. (11). The logic of this choice is that one electron is thereby allowed to reach the reaction surface $\mathcal{S}$ in any channel for which at least one open-type two-electron basis vector is included, but in no channel are *both* electrons able to move beyond r_0 simultaneously. As in usual MQDT treatments, only one electron escape beyond the reaction surface is considered here. In practice two open-type two-electron basis vectors $|y_k^o\rangle$ defined in the above fashion are included for each MQDT channel, while many more closed-type $|y_k^c\rangle$ are included. (As was discussed in detail in Ref. [8(b)], the closed-type basis set vanishing at r_0 is complete by itself, in the ordinary sense of quantum mechanics. Yet extra flexibility is provided, for describing general bound and continuum wave functions that fail to vanish at $r=r_0$, by including these open-type basis vectors. But as a rule of thumb the open-type basis should be kept comparatively small so that the basis does not become linearly dependent to within the machine precision. Experimentation with one to three open-type basis vectors per channel has shown little sensitivity to this number, and most eigenchannel R-matrix calculations presently use two per channel.) If for a given set of $\{n_1l_1j_1l_2j_2\}$, only closed-type radial orbitals $u_{n_2l_2j_2}(r)$ are included in the full basis set, the channel $i\equiv\{n_1l_1j_1l_2j_2\}$ is called "strongly closed," while the presence of an open-type orbital $u_{\bar{n}_2l_2j_2}(r)$ in the full basis signifies that the corresponding channel i to be treated as open or weakly closed in the eventual MQDT calculation.

B. Streamlined solution of the generalized eigensystem

After the basis set is designed and all matrix elements calculated, Eq. (5) can be solved numerically at each desired energy E. The jj-coupled calculations presented in this paper typically involve 200 to 500 basis functions for any given J, depending on factors such as the value of r_0, the values of J and parity, the number of channels, and the degree of convergence desired. For such large basis sets the solution of the linear eigensystem (5) at many energies can become time consuming, and for this reason a much more efficient "streamlined" solution method of Greene and Kim [8(b)] is used.

For a modest box size r_0 less than about 25 a.u., good convergence is achieved using eight closed-type basis vectors per channel and two open-type vectors per channel. The calculations here involved typically five to 15 open or weakly closed channels, with an additional 100 to 300 strongly closed two-electron basis vectors included to improve the flexibility of the basis set to describe various polarization and correlation effects. Thus the total variational basis set breaks up into mostly closed-type basis vectors with perhaps an order of magnitude fewer open-type vectors. It is this fact that the streamlined formulation takes advantage of, by partitioning the matrices in Eqs. (5)–(8) into open and closed partitions, e.g.,

$$\underline{\Gamma}=\begin{bmatrix}\underline{\Gamma}^{cc} & \underline{\Gamma}^{co}\\ \underline{\Gamma}^{oc} & \underline{\Gamma}^{oo}\end{bmatrix}, \tag{12}$$

and

$$\underline{\Lambda}=\begin{bmatrix}0 & 0\\ 0 & \underline{\Lambda}^{oo}\end{bmatrix}. \tag{13}$$

This partitioning breaks Eq. (5) into two coupled matrix equations,

$$\underline{\Gamma}^{cc}\mathbf{Z}^c+\underline{\Gamma}^{co}\mathbf{Z}^o=0\ , \tag{14}$$

and

$$\underline{\Gamma}^{oc}\mathbf{Z}^c+\underline{\Gamma}^{oo}\mathbf{Z}^o=b\underline{\Lambda}^{oo}\mathbf{Z}^o\ . \tag{15}$$

Using (14) to eliminate $\mathbf{Z}^c$ from (15) leads to a matrix equation of much smaller dimension for $\mathbf{Z}^o$, specifically

$$[\underline{\Gamma}^{oo}-\underline{\Gamma}^{oc}(\underline{\Gamma}^{cc})^{-1}\underline{\Gamma}^{co}]\mathbf{Z}^o=b\underline{\Lambda}^{oo}\mathbf{Z}^o\ . \tag{16}$$

Inversion of the matrix $\underline{\Gamma}^{cc}$ at many energies E is efficiently accomplished by first transforming the closed-portion of the basis set into the energy-independent representation in which $\underline{H}^{cc}$ is diagonal, with eigenvalues E_λ and orthonormal eigenvectors $X_{k\lambda}$. (Here we have used the facts that $\underline{O}^{cc}$ is the unit matrix and that $\underline{L}^{cc}$ vanishes for our present choice of basis set.) Using $\underline{\Omega}$ to denote the matrix in square brackets in Eq. (16), its energy dependence is now given analytically

$$\Omega_{kk'}=2(EO^{oo}_{kk'}-H^{oo}_{kk'}-L^{oo}_{kk'})-2\sum_\lambda\frac{(EO^{oc'}_{k\lambda}-H^{oc'}_{k\lambda}-L^{oc'}_{k\lambda})(EO^{c'o}_{\lambda k'}-H^{c'o}_{\lambda k'}-L^{c'o}_{\lambda k'})}{E-E_\lambda}\ . \tag{17}$$

In Eq. (17) the notation c' implies that the closed portion of the two-electron basis set is now in the transformed representation, i.e., $O^{oc'}_{k\lambda}=\sum_{k'}O^{oc}_{kk'}X_{k'\lambda}$, $O^{c'o}_{\lambda k}=\sum_{k'}O^{co}_{k'k}X_{k'\lambda}$, etc. The semianalytic energy dependence of all matrices in (16), combined with the much smaller number of open-type than closed-type basis vectors, thus makes (16) much faster to solve on a fine-energy mesh than the original Eq. (5).

Recalling that the dimension of the reduced equation (16) is $2N_o$, where N_o is the number of open and weakly

closed channels in the calculation, this generalized eigenvalue equation has N_o nontrivial eigenvalues b_β and corresponding eigenvectors $Z^o_{k\beta}$ at each energy E. The component $\psi_{i\beta}$ of the βth eigenstate in the ith channel can be written as

$$\psi_{i\beta}=\sum_{\bar{n}_2} Z^o_{i\bar{n}_2,\beta} u_{\bar{n}_2 l_{2i} j_{2i}}(r_0) , \tag{18}$$

where we use the notation $k\equiv\{i\bar{n}_2\}$ for the open portion of the variational two-electron basis set. The function $u_{\bar{n}_2 l_{2i} j_{2i}}(r)$ denotes the radial part of an open-type one-electron eigenfunction $|\bar{n}_2(sl_{2i})j_{2i}\rangle$ as described in Sec. II A above. The radial derivative of this same solution is then simply $\psi'_{i\beta}=-b_\beta\psi_{i\beta}$. By matching $\psi_{i\beta}$ and its derivative to a linear combination of regular and irregular Coulomb functions (f_i,g_i) in the ith channel, one obtains the usual "smooth" reaction matrix $K_{ii'}$ of MQDT, and the relevant dipole matrix elements needed for a photoionization calculation also (Eqs. (13)–(17) of Ref. [7(a)], for instance). In the calculations presented below, the value of r_0 typically was chosen in the range of 18 to 20 a.u.

III. RESULTS OF THE CALCULATIONS

A. Absorption spectra of Sr, Ba, and Ra

In this section we analyse the limitations of the approximations inherent in the *jj*-*LS* frame transformation by comparing the results previously obtained with *LS*-coupled *R*-matrix calculations and the *jj*-*LS* frame transformation for the absorption spectra of Sr [6(a)] and of Ba [14] with those obtained in the present work by performing *R*-matrix calculations in *jj* coupling. In addition, new *R*-matrix results obtained for Ra will be presented. These latter results deal with not only the photoionization spectrum, but also with the $J=1$ odd-parity bound spectrum.

R-matrix calculations performed either in *LS* coupling or *jj* coupling to investigate the absorption spectrum below the $m_0p_{3/2}$ threshold of Sr ($m_0=5$), Ba ($m_0=6$), and Ra ($m_0=7$) include 13 odd-parity $J=1$ channels, which are the *jj*-coupled ionization channels involved in the MQDT calculation of observables. [These channels are $m_0snp_{1/2}, m_0snp_{3/2}$, $(m_0-1)d_{3/2}np_{1/2}$, $(m_0-1)d_{3/2}np_{3/2}$, $(m_0-1)d_{3/2}nf_{5/2}$, $(m_0-1)d_{5/2}np_{3/2}$, $(m_0-1)d_{5/2}nf_{5/2}$, $(m_0-1)d_{5/2}nf_{7/2}$, $m_0p_{1/2}ns$, $m_0p_{1/2}nd_{3/2}, m_0p_{3/2}ns, m_0p_{3/2}nd_{3/2}, m_0p_{3/2}nd_{5/2}$.] Theoretical predictions for Sr and Ba will be compared with the most recent experimental data. In particular, we will consider the new experimental photoionization spectra obtained for Sr and Ba by Griesmann, Esser, and Hormes [16] using synchrotron radiation. The results obtained with *R*-matrix calculations in *LS* and *jj* coupling will be referenced throughout this paper as *LS* and *jj* results, respectively. However, the reader must keep in mind that *R*-matrix calculations performed in *LS* coupling are combined with MQDT calculations, including fine-structure effects through a frame transformation. Although all photoionization cross sections have been calculated using both the length and velocity forms, only velocity results are presented here, except in one case. In general, the agreement between length and velocity calculations is comparable to that shown later in Fig. 4, although it is somewhat poorer for the radium calculations.

1. Strontium

Figure 1 compares the experimental results [16] obtained in Sr below the $4d_{3/2}$ threshold with the *jj* results. The measurement of Griesmann, Esser, and Hormes [16] is not absolute. To compare it with our results, we have normalized the experimental curve by adjusting the peak photoionization cross section of the dominant resonance, namely the $4d6p\ ^1P$ resonance around 196 nm. Assignments of the other resonant states $4dnp$, $4dnf$, and $5p6s$ $J=1$ can be found in Refs. [6(a)] and [22]. The overall agreement between experiment and theory is better than that previously obtained [6(a)] by performing the variational calculation in *LS* coupling. However, the improvements are not due to the different treatment of the spin-orbit interaction but derive instead from three other differences. First, the one-electron model potential $V(r)$ used in Ref. [6(a)] had a very simple form involving only three parameters, while the new *jj* calculations are done with a more sophisticated model potential including *l*-dependent screening and polarization terms. As a result the theoretical energy levels of Sr^+ are more accurate here than in Ref. [6(a)]. Second, inaccuracies occur in MQDT calculations conducted following the *LS*-coupled *R*-matrix calculation in the low-energy range when experimental one-electron energies (including the fine-structure splitting) are used for the MQDT threshold energies. Difficulties arise when some channels are "strongly closed" but treated as "weakly closed" in the *R*-matrix calculation. In fact, during the matching procedure on

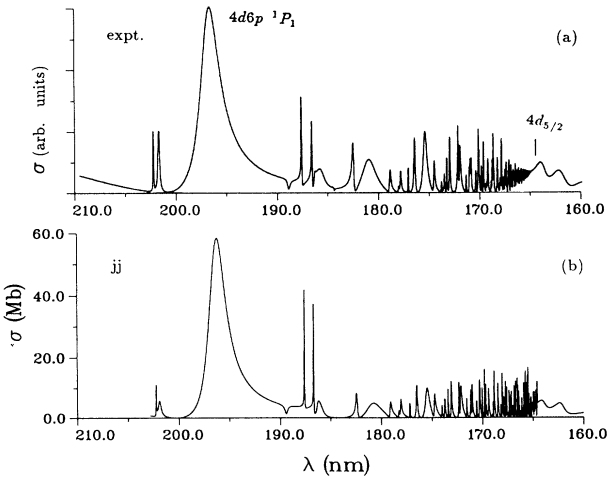

FIG. 1. Photoabsorption spectrum of Sr in the wavelength region from 210 to 160 nm, below the $4d_{5/2}$ threshold: total photoionization cross section. (a) Relative measurement of Griesmann, Esser, and Hormes [16] (wavelength resolution ~0.05 nm). (b) *jj* results.

the reaction surface which gives the K matrix, the Coulomb functions are evaluated with theoretical photoelectron energies, the fine structure of the thresholds being neglected at this point but accounted for later in the MQDT calculation. At the low-energy end in each channel, the MQDT parameters acquire a strong energy dependence and the MQDT results become very sensitive to the value of the threshold energy. This point has been discussed by Greene and Kim [7(a)], and will be documented later in the following sections. It was found [14] in Ba that these difficulties can be removed by using theoretical energies instead of experimental ones for the threshold energies associated with some strongly closed channels. In Ref. [6(a)], the use of experimental energies for the $5p_{1/2,3/2}$ thresholds led to inaccuracies in the energy range corresponding to the lowest end of the $5pns$, nd series, although use of experimental threshold energies definitely improves the calculation near those thresholds. It is to be stressed that these difficulties inherent in the frame-transformation approximation are almost absent when R-matrix calculations are done in jj coupling because then the experimental and theoretical threshold energies are very close. Finally, the previous R-matrix calculations [6(a)] were carried out with a small two-electron basis set, whereas the present jj-coupled R-matrix calculation introduces an enlarged basis set, improving the convergence of the variational calculation.

Figure 2 compares experimental [16] and theoretical photoionization cross sections of Sr at higher energies, between the $4d_{5/2}$ and $5p_{3/2}$ thresholds. In this energy range, the jj results, curve 2(b), are very similar to those previously obtained in the LS calculations [6(a)]. The comparison of experiments with the results obtained with LS-coupled R-matrix calculation is discussed further in Ref. [6(a)].

2. Barium

The eigenchannel R-matrix calculation performed in jj coupling for the absorption spectrum of Ba uses the same model potential $V(r)$ as in the previous calculations [14] done in LS coupling. Moreover, the basis sets used in both calculations are very similar. Thus, the comparison of theoretical predictions of the two different treatments furnishes a more stringent probe of the frame-transformation approximation.

Figure 3 compares the LS [14] and jj-photoionization cross sections, calculated between the $6s$ and $5d_{3/2}$ thresholds, with the observations of Griesmann, Esser, and Hormes [16]. It is evident from Fig. 3 that R-matrix calculations in either LS or jj coupling are almost identical. For the reasons outlined above, the spin-orbit-averaged theoretical energy was used for the $6p_{1/2,3/2}$ threshold in the MQDT calculation done with the K matrix deduced from the LS-coupled R-matrix calculation. Various minor discrepancies between the LS results and experiment, detailed in Ref. [14], have not been removed by performing the R-matrix calculation in jj coupling. The structure of the autoionizing odd-parity $J=1$ spectrum below the $5d_{3/2}$ threshold is due to the $5dnp$ and $5dnf$ resonances. This spectrum has been recently reinvestigated using laser spectroscopy by Gounand *et al.* [23], the $5dnlJ=1^o$ levels being excited from the $5d^2\,{}^1S_0$

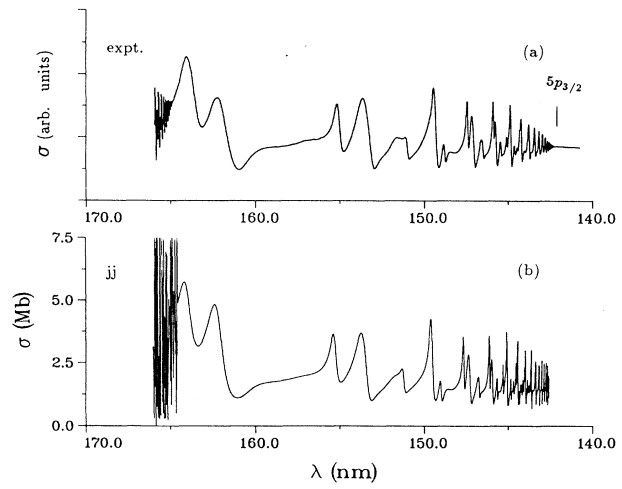

FIG. 2. Same as Fig. 1 in the wavelength region from 166 to 143 nm, between the $4d_{5/2}$ and $5p_{3/2}$ thresholds.

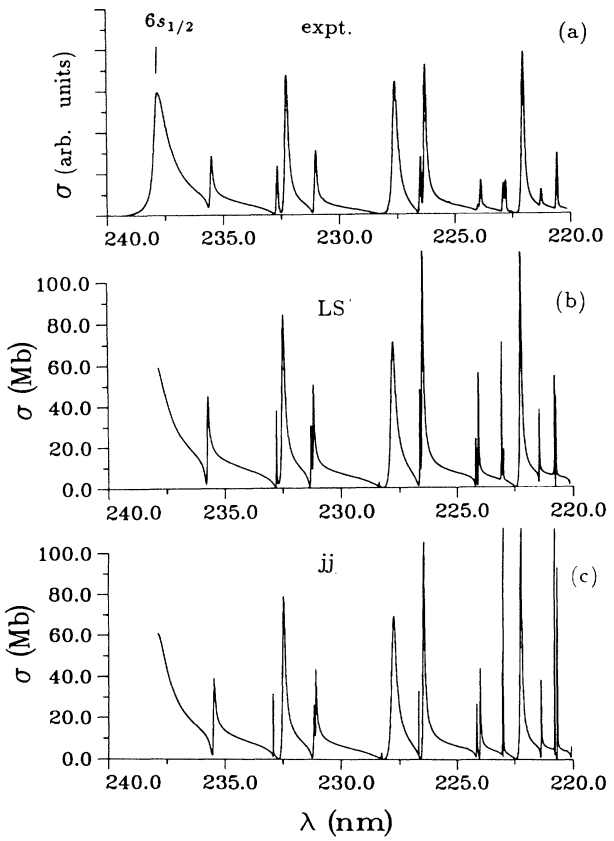

FIG. 3. Photoabsorption spectrum of Ba in the wavelength region from 240 to 220 nm, below the $5d_{3/2}$ threshold: total photoionization cross section. (a) Relative measurement of Griesmann, Esser, and Hormes [16] (wavelength resolution ~0.05 nm). (b) LS results. (c) jj results.

level; in addition, the assignments of the observed resonances deduced from the R-matrix calculation [14] are presented in Ref. [23].

The experimental results obtained in Ba by Brown and Ginter [24] just below the $6p_{1/2}$ threshold are compared with R-matrix results in Fig. 4. The LS and jj results are here again almost identical, both calculations reproducing the experimental spectrum accurately. Here curves 4(b) and 4(c) display both length and velocity results which are very close, giving some confidence in the convergence of the variational calculations.

3. Radium

Radium involves a much stronger spin-orbit interaction than Ba and thus the comparison of R-matrix results obtained in either LS or jj coupling is of particular interest for analyzing the limitations of the frame transformation for describing spin-orbit effects. The $J=1$ odd-parity spectrum of Ra is largely unknown experimentally, however, as the only available data besides that compiled by Moore [18] concerns the $7snp\ ^1P_1$ principal series observed by Tomkins and Ercoli and analyzed by Armstrong, Wynne, and Tomkins [19]. We first consider how these data relevant to the bound spectrum are described by R-matrix calculations, after which we will present R-matrix predictions for the photoionization spectrum.

(a) $J=1$ odd-parity bound spectrum of Ra. The $J=1$ odd-parity spectrum of Ra is much simpler than the homologous spectrum of Ba since only three doubly excited states appear, while in Ba 12 doubly excited levels lie below the first ionization limit. The three doubly excited levels perturbing the $7snp\ ^{1,3}P_1$ Rydberg series of Ra are the $6d7p\ ^3D_1$, $^3P_1$, and $^1P_1$ levels. The two former levels appear in the table of Moore[18] while the last one has not been observed. Two previous two-channel MQDT calculations have been carried out to analyze the perturbation of the $7snp\ ^1P$ series by the $6d7p\ ^1P$ level. The first analysis was the empirical treatment of Armstrong, Wynne, and Tomkins [19]. The second, performed by Kim and Greene [25], used an eigenchannel R-matrix calculation in LS-coupling and ignored fine-structure effects altogether. In both studies, the classification of low-lying levels was questioned.

We have performed two different R-matrix calculations, namely a five-channel treatment in LS coupling, including the $7snp$ and $6dnp$ $J=1$ channels, and a 13-channel treatment in jj coupling, introducing in addition the $6dnf$, $7pns$, and $7pnd$ $J=1$ channels. These latter channels do not support any bound level and have accordingly been treated as strongly closed in the LS calculation. Figure 5 displays the theoretical Lu-Fano plots showing $-\nu_{7s}$ (mod 1) vs $\nu_{6d_{3/2}}$ (ν_{7s} and $\nu_{6d_{3/2}}$ are the

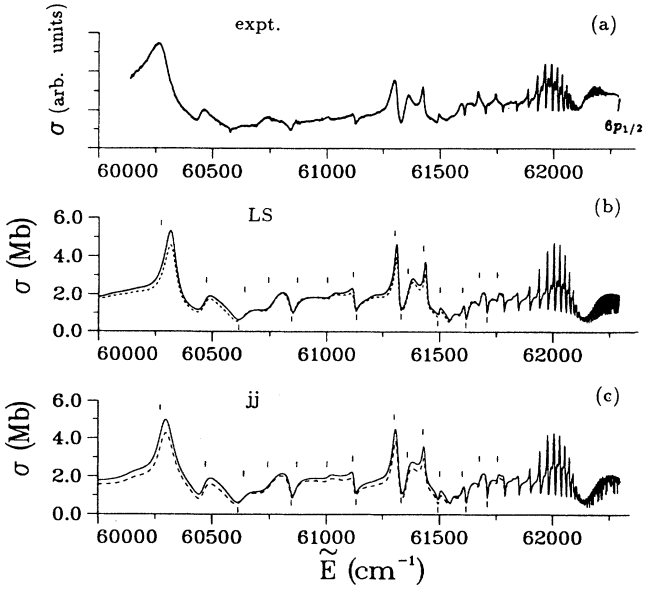

FIG. 4. Photoabsorption spectrum of Ba in the energy range from 60 000 cm^{-1} to the $6p_{1/2}$ threshold: total photoionization cross section. (a) Relative measurement of Brown and Ginter [24] (energy resolution $\sim 0.11\ cm^{-1}$). (b) LS velocity (——) and length results (— — —); vertical bars indicate the position of the observed absorption peaks and minima. (c) jj velocity (——) and length results (— — —).

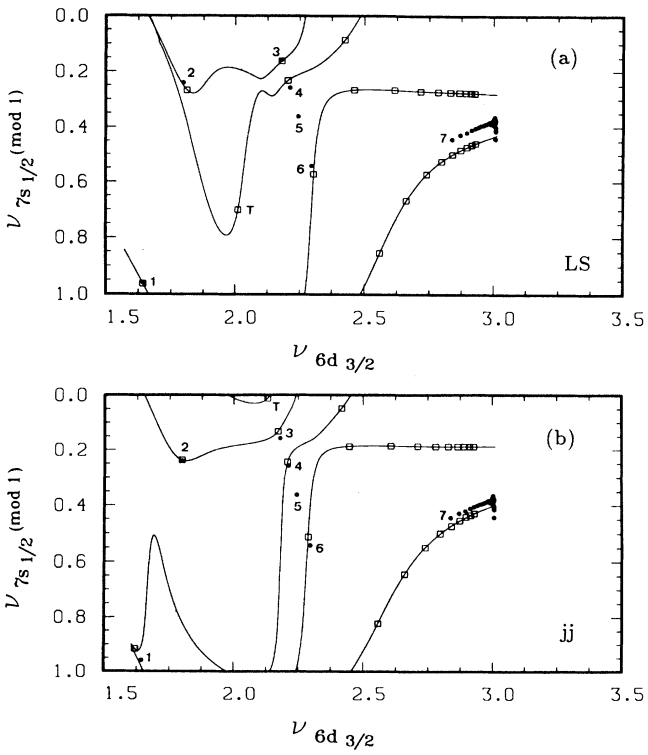

FIG. 5. Lu-Fano plot of the $J=1$ odd-parity bound levels of Ra in the $-\nu_{7s}$ (mod 1) against $\nu_{6d_{3/2}}$ plane. (a) ——, LS calculation; ●, experimental level positions [17–19]: (1) $7s7p\ ^3P_1$, (2) $7s7p\ ^1P_1$ (3)–(6) see the text, (7) $7s13p\ ^1P_1$; □, theoretical level positions [for (T) see the text]. (b) ——, jj calculation.

effective quantum numbers relative to the $7s$ and $6d_{3/2}$ thresholds). Curves 5(a) and 5(b) compare the LS and jj results, respectively, with the known levels [17–19]. The low-lying $7s7p\ ^{1,3}P$ levels [18] and the high-lying $7snp\ ^1P$ levels [19] ($n \geq 13$) agree well with our calculated values, a better description of high-lying levels being obtained with jj calculation. Discrepancies occur in the intermediate-energy range, however, with level number (5) being far from each theoretical curve. However, in this energy range the two theoretical curves are rather different and both support one theoretical energy level (labeled by T) which cannot be associated with any experimental level. The energy value predicted by the jj calculation is 30477 cm^{-1}. Four levels, namely the $7s8p\ ^{1,3}P$ levels and $6d7p\ ^3D$, ^3P levels, are expected to lie in the range $2.0 \leq \nu_{6d_{3/2}} \leq 2.5$ in agreement with our predictions. The four levels are so intermixed that it is not possible to unambiguously label them, except in the case of level number (6) for which the calculations seem to confirm the classification of Russell [17] adopted by Moore [18], namely $6d7p\ ^3P$. Additional experimental investigations would help greatly to sort out this problem and provide a decisive judgment on the accuracy of the present calculations. Our prediction for the $6d7p\ ^1P$ level, at 37 855 cm^{-1}, based on the jj calculation, is close to previous semiempirical predictions [19] (37 895–38 048 cm^{-1}).

Some more points should be discussed here. Our calculations show the oscillator strengths of the $7s^2$–$7snp\ ^3P$ series are considerably weaker than those of the $7s^2$-$7snp\ ^1P$ series, by a factor of about 800 for $n \geq 13$ in the jj calculation. It is surprising that the triplet states are so weakly excited from the ground state, considering the strength of the radium spin-orbit interaction. But this result is consistent with the fact that the triplet $7snp\ ^3P$ series has not been observed in absorption measurements from the ground state. It must be noted that the triplet $m_0snp\ ^3P$ series of the lighter alkaline earths have not been observed from the ground state either, but that is less surprising owing to the smaller spin-orbit interaction. Multistep laser investigation, as performed in Ca, Sr, and Ba [12], would be desirable to extend our knowledge of the Ra spectrum, although its radioactivity clearly causes additional experimental difficulties. Unlike Ba, oscillator strengths of the principal series of Ra behave very regularly in the high-energy range because no perturber occurs there.

One major feature in all the heavy alkaline-earth atoms is the occurrence of a very strong interaction between the m_0snp and $(m_0-1)dnp\ ^1P$ channels; just as for Ca [7(a)], Sr [6(b)], and Ba [14], the corresponding channels of Ra are almost equally mixed at the m_0s threshold, the channel-mixing angle around 0.2π being close to the theoretical maximum 0.25π. [The channel-mixing angle θ is defined for a two-channel system in MQDT as the rotation angle needed to transform the reaction matrix into its diagonal representation. An arbitrary mixing angle θ can be transformed into the range $-\pi/4 \leq \theta \leq \pi/4$ by using the fact that the transformation $\theta \rightarrow \theta + n\pi$ simply multiplies each eigenstate of the reaction matrix by $(-1)^n$, and also by using the fact that the transformation $\theta \rightarrow \pi/2 - \theta$ amounts to interchanging the arbitrary ordering of the eigenstates.] This near invariance of the channel mixing, discussed by Wynne and Armstrong [26], was used by Armstrong, Wynne, and Tomkins [19] to predict the locations of unobserved Ra levels.

(b) Absorption spectrum of Ra. Figure 6 compares cross sections for photoionization of ground state Ra obtained below the $6d_{3/2}$ threshold using R-matrix calculations in LS and jj coupling. Curves 6(a) and 6(b) display marked differences in the whole energy range. Both MQDT calculations introduce 13 channels. In addition, an eight-channel R-matrix calculation in LS coupling was carried out in which the $6pns,nd$ channels were treated as strongly closed and omitted from the MQDT calculation. The corresponding result is almost identical to curve (b) in Fig. 6, thus excluding the possibility that differences between curves 6(a) and 6(b) might result from inaccuracies in the treatment of the strongly closed channels converging to the $6p$ thresholds. The autoionizing structures in this energy range are due to $6dnp$ ($n \geq 8$) and $6dnf$ $J=1$ resonances and perhaps to $7p8s$ $J=1$ resonances which are likely to lie below the $6d_{3/2}$ threshold. The resonances appear to be so intermixed that we have not attempted to identify them.

The LS and jj results obtained for the photoionization cross sections between the $6d_{5/2}$ and $7p_{3/2}$ thresholds are compared in Fig. 7. In this energy range, clearly curves 7(a) and 7(b) bear a much closer resemblance than in the lower-energy range. However, differences, mainly near the strong resonant peak around 60 000 cm^{-1}, are much more visible than in Figs. 3 and 4 corresponding to Ba. Here again we have not attempted to identify the predicted structures due to transitions to the $7pns$ and $7pnd$ levels. Since the resonances are very broad and overlapping, it is almost certain that, just as for the homologous reso-

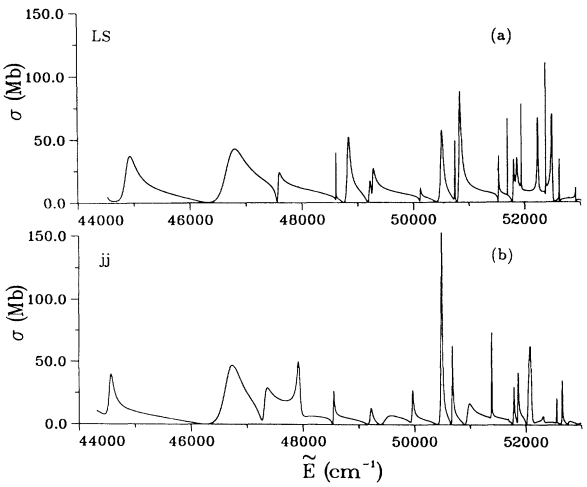

FIG. 6. Total photoionization cross section of ground-state Ra in the energy range from 44 000 to 53 000 cm^{-1}, below the $6d_{3/2}$ threshold. (a) LS results. (b) jj results.

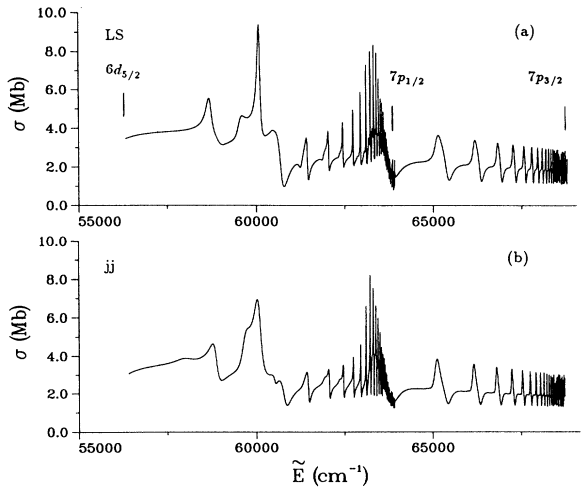

FIG. 7. Same as Fig. 6 in the energy range between the $6d_{5/2}$ and $7p_{3/2}$ thresholds.

nances of Ba [14], an independent particle label is meaningless for most of them.

It is worth noting that the autoionization pattern predicted for Ra above the $6d_{5/2}$ threshold presents many similarities with that observed for Ca, Sr, and Ba in the corresponding energy range. Below the $7p_{1/2}$ threshold, the structures with periodic enhancement due to low-lying $7p_{3/2}nl$ levels mixed with Rydberg levels $7p_{1/2}nl$ bear much resemblance to the structures observed in Ba (see Fig. 4) and in Sr (see Fig. 9 of Ref. [6(a)]). In the same way, the periodic pattern of asymmetrical absorption profiles predicted between the $7p_{1/2}$ and $7p_{3/2}$ thresholds is very similar to that observed near the m_0p thresholds of Sr [6(a)], Ba [14], and even Ca [7(a),7(b)]. These marked similarities throughout the heaviest alkaline earths reflect the systematic near invariance of the electronic channel mixings. Here, the strongest channel mixing in all the heavy alkaline-earth atoms corresponds to the $m_0p\epsilon d$-$(m_0-1)d\epsilon f$ mixing. From Figs. 1, 3, and 6, it is evident that below the $(m_0-1)d$ threshold there is much less evidence for near invariance in electronic channel mixing, although much of this difference in appearance is due to the variation of the threshold splitting $(m_0-1)d-m_0p$ in these atoms.

The large differences between curves (a) and (b) of Fig. 5 clearly suggest some limitations of the frame transformation to account for spin-orbit effects in Ra. To understand these limitations, recall that the term "frame transformation" in this paper implies the following procedure. First, *LS*-coupled reaction matrices are obtained variationally, neglecting all spin-orbit interactions. Second, these *LS*-coupled matrices are recoupled by a geometric *jj*-*LS* transformation to give a single *jj*-coupled reaction matrix. (It is easy to show that this recoupling, by itself, will have no effect on the spectrum whatsoever if the initial-state calculation ignores fine-structure interactions, and if *j*-independent thresholds are used in the MQDT calculation.) The third step is to perform the quantum-defect calculation on a fine-energy grid, but *including the experimental j-dependent spin-orbit splitting* of the inner electron threshold energies. This last step is the only one which uses ion-dependent information about the spin-orbit interaction, but it has a major qualitative effect at energies close to fine-structure-split thresholds. Accordingly, the frame transformation accounts mainly for the spin-orbit interaction of the inner electron, while it is neglected for the outer excited electron except through effects associated with energy conservation. A good measure of the core-electron spin-orbit interaction is the difference between the quantum defects of spin-orbit-split doublet-ion levels. For the m_0p ion core, $\Delta\mu=0.045$ and 0.12 for Ba^+ and Ra^+, respectively, while for the $(m_0-1)d$ ion core one has $\Delta\mu=0.012$ and 0.030. It is much more difficult to estimate the strength of the spin-orbit interaction for the outer electron, but it is clear that this is far stronger for the *np* electrons involved in $(m_0-1)dnp$ levels in Ra than in the lighter alkaline earths. Part of the difference between curves (a) and (b) in Fig. 5 is thus likely to result from the incomplete treatment of the spin-orbit interaction by the *jj*-*LS* frame transformation. Moreover, below the 6*d* threshold the energy dependence of the MQDT parameters is stronger than above, and thus the results are much more sensitive to the values of the threshold energies used in the MQDT calculation than are the results above the 6*d* threshold. The spin-orbit interaction strength of *nd* electrons in the 7*pnd* levels of Ra is likely to be of the same order of magnitude as that of *np* electrons in the 5*dnp* levels of Ba. But no difference occurs between curves (b) and (c) of Fig. 3, while some are visible in Fig. 6. These differences probably result from the fact that the fine-structure splitting of the 7*p* level of Ra^+ is three times larger than the splitting of the 5*d* level of Ba^+.

No experimental spectrum is available in this energy for Ra and thus the reliability of the predictions remains to be tested. In particular, one major open question is whether the present *jj*-coupling calculation adequately accounts for relativistic effects beyond the spin-orbit interaction. As argued elsewhere [15], these are described at least approximately through the use of a semiempirical model potential $V(r)$, but this approximation has not yet been adequately tested in an atom as heavy as radium.

B. $J=0$ and 2 even-parity spectra of Ba below the $5d_{3/2}$ threshold

This section deals with the $J=0$ and 2 even-parity spectra of Ba, which have been extensively investigated since the advent of laser spectroscopy. In addition to experimental investigations making a term analysis [27,28] high-resolution laser studies have been used to probe the detailed structures and properties of Rydberg levels and doubly excited autoionizing levels. Most of the pioneering investigations dealt with the perturbations of the $6sns\ ^1S_0$ and $6snd\ ^{1,3}D_2$ series by low-lying doubly excited states. Perturbations are reflected not only by level structure but also by lifetimes, hyperfine structure, Landé *g* factors, and various other observables (see Ref. [4] and references therein). Now the focus has shifted toward the

autoionizing Rydberg states, experiments having revealed interesting properties such as the extreme stability [29] of some levels.

The MQDT has enjoyed remarkable success in describing the experimental data. However, previous analyses have utilized empirical MQDT parameters which are adjusted to agree with a particular set of measurements. The complexity of Ba is such that these empirical treatments encounter serious difficulties relating to the energy dependence of the parameters, to the occurrence of isolated perturbers, and to the sometimes overwhelming number of interacting channels [4]. The previous empirical analyses devoted to bound spectra [27,30] were achieved using the eigenchannel MQDT formalism [3(b)], whereas now the phase-shifted reaction-matrix approach [3(c)] is currently used in the autoionizing region, although this is purely a matter of convenience.

It is of particular interest to analyse how the eigenchannel R-matrix approach is able to handle the bound spectrum of Ba, in particular the complicated $J=2^e$ spectrum investigated so extensively in previous works. The empirical MQDT treatments showed large departures from the geometric jj-LS frame transformation. R-matrix calculations performed in the present work for the $J=0^e$, $J=2^e$ bound spectra, in both LS and jj coupling, should shed light on whether these departures are due to the spin-orbit interaction or to the approximations used to simplify the fitting of empirical MQDT parameters. Moreover, by overcoming the limitations of empirical MQDT, it should be possible to get new insight into the nature of channel mixing and to check the assignments of levels, especially in cases where the term designation has been controversial.

In the autoionizing region, the new R-matrix results presented below will concern the $5dnl$ $J=0^e$ and $J=2^e$ autoionizing Rydberg series and the $6p^2\,{}^1S_0$ level, excited from either the $6s6p$ or else the $5d6p\,{}^1P_1$ bound level. Here again calculations are conducted in both LS and jj coupling.

1. $J=0$ even-parity bound spectrum

The $J=0^e$ spectrum consists of the $6sns\ {}^1S_0$ Rydberg series and of six doubly excited levels, low-lying members of Rydberg series converging to the $5d_j$ or $6p_j$ thresholds. Five-channel R-matrix and MQDT calculations are carried out. The jj-coupled ionization channels are $6s_{1/2}ns_{1/2}$, $5d_{3/2}nd_{3/2}$, $5d_{5/2}nd_{5/2}$, $6p_{1/2}np_{1/2}$, and $6p_{3/2}np_{3/2}$. Identifications of the observed levels were based on an empirical four-channel MQDT treatment [27] involving only one $6pnp$ channel introduced to take care of the $6p^2\,{}^3P_0$ bound level.

Figure 8 compares the theoretical Lu-Fano plots to experiment, curves 8(a) and 8(b) showing the LS and jj results, respectively. To avoid inaccuracies at the low-energy end of the $6pnp$ channels, the theoretical $6p_{1/2,3/2}$ threshold energy is used in the MQDT calculation conducted following the R-matrix calculation in LS coupling. The dots correspond to experimental data [18,27,31]. For $n \geq 30$, the very precise energy values measured by Neukammer *et al.* [31] are plotted instead of those given in Ref. [27]. Note that a recent experiment [23] has confirmed that the $5d^2\,{}^1S_0$ level [32] lies at 25 873.83 cm^{-1}. The curves of Fig. 8 have to be compared with Fig. 4 of Ref. [27] which, however, does not include the low-energy levels for $\nu_{5d_{3/2}} \leq 2.9$. Both R-matrix calculations correctly reproduce the perturbations of the $6sns$ series by the $5d6d\ {}^3P_0$, $5d6d\ {}^1S_0$, $5d7d\ {}^3P_0$, and $6p^2\,{}^3P_0$ levels, the jj results being closer to experiment. The description of the low-lying $5d^2$ levels is less satisfying; note that theoretical curves 8(a) and 8(b) are quite different in the low-energy range, a point which is discussed in Sec. IV. One key result of the calculations concerns the assignment of the various levels: the present study completely confirms the identifications deduced from empirical MQDT analysis [27]. The classifications of some levels are still questioned [26,33] but we hope this study will close the controversy.

2. $J=2$ even-parity bound spectrum

The $J=2^e$ bound spectrum is much more complicated than the $J=0^e$ spectrum, since it involves 16 doubly excited levels pertaining to $5dnd$ ($n=5$–7), $5dns$ ($n=7,8$),

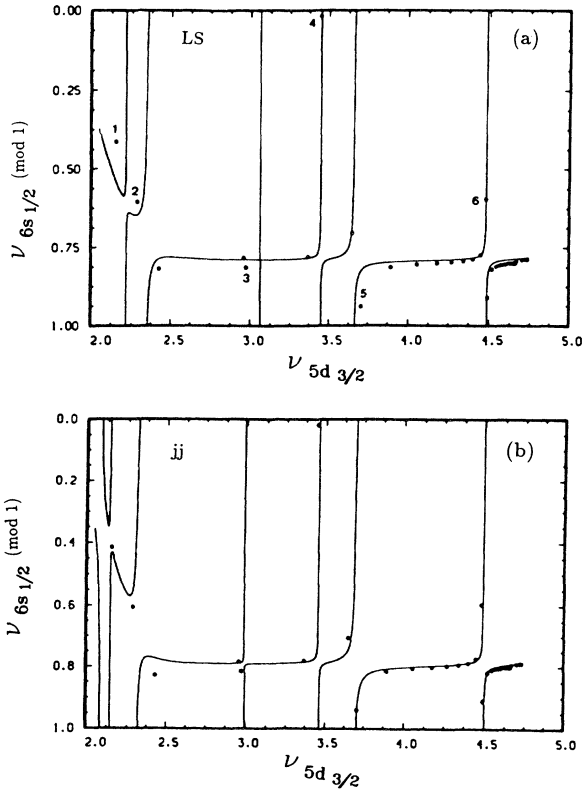

FIG. 8. Lu-Fano plot of the $J=0$ even-parity bound levels of Ba in the $-\nu_{6s}$ (mod 1) against the $\nu_{5d_{3/2}}$ plane. (a) ——, LS calculation; ●, experimental level positions [18,27,31]: (1) $5d^2\,{}^3P$, (2) $5d^2\,{}^1S$, (3) $6p^2\,{}^3P$, (4) $5d6d\,{}^3P$, (5) $5d6d\,{}^1S$, (6) $5d7d\,{}^3P$; (b) ——, jj calculation.

and $6p^2$ configurations which perturb in several places the $6snd\ ^1D_2$ and $^3D_2$ Rydberg series. The R-matrix and MQDT calculations are conducted using 11 channels. The jj-coupled channels are as follows: $6s_{1/2}nd_{3/2}$, $6s_{1/2}nd_{5/2}$, $5d_{3/2}ns_{1/2}$, $5d_{3/2}nd_{3/2}$, $5d_{3/2}nd_{5/2}$, $5d_{5/2}ns_{1/2}$, $5d_{5/2}nd_{3/2}$, $5d_{5/2}nd_{5/2}$, $6p_{1/2}np_{3/2}$, $6p_{3/2}np_{1/2}$, and $6p_{3/2}np_{3/2}$. This spectrum was analyzed previously [30] by an empirical nine-channel MQDT treatment which disregarded the $6p^2\ ^3P_2$ level and introduced only one $6pnp$ channel to account for the $6p^2\ ^1D_2$ level. Later, experimental data on Landé g factors and hyperfine structure have permitted improvements on the initial MQDT model which had been derived from energies [4] alone.

Figure 9 compares the theoretical Lu-Fano plots with experimental data [18,27,31,34]. Note that the low-lying $6s5d\ ^{1,3}D_2$ levels fall below the energy range considered in the present study. Here again curves 9(a) and 9(b) correspond, respectively, to the LS and jj results. As in the $J=0^e$ case, both Lu-Fano plots differ in the low-energy range where the MQDT parameters have a strong energy dependence. These curves are to be compared with Fig. 1 of Ref. [30], which, however, does not consider the low-lying levels. There, the points were exactly on the curve, whereas some deviations are visible here. However, the agreement between theory and experiment is generally quite satisfying, accounting for the great complexity of the spectrum despite some noticeable discrepancies. We have numbered the doubly excited levels as well as some $6snd$ levels, whose assignment will be discussed later. The calculations correctly reproduce the perturbations due to the $5d^2\ ^3F_2$, $^1D_2$, $^3P_2$ (1,2,3), $5d6d\ ^3D_2$, $^3F_2$, $^1D_2$, $^3P_2$ (8,9,11,12), and $5d7d\ ^3D_2$, $^3F_2$, $^1D_2$ (16,17,18) levels. The perturbations due to the $5dns\ ^3D_2$, $^1D_2$ levels (4 and 5 for $n=7$; 14 and 15 for $n=8$) are also well described. The R-matrix calculations permit the previous assignment of levels to be checked. Only a few levels, as detailed below, were misclassified in Ref. [30]. The levels listed above were correctly assigned in Ref. [30]. In contrast, in the intermediate-energy range where there are more perturbers than there are $6snd$ levels, our calculations suggest a reclassification of levels 6, 10, and 13 as indicated in Table II. This new classification is close to the original one given by Moore [18]. It is worth noting that several experiments [33] have shown recently that levels 6 and 7 are predominantly $6p^2$ in character, in harmony with our new classification. One must keep in mind that no level corresponds actually to an independent-electron configuration: the $6p^2$ levels interact strongly with nearby levels, and in the higher-energy range several doubly excited levels are strongly mixed with dense Rydberg levels.

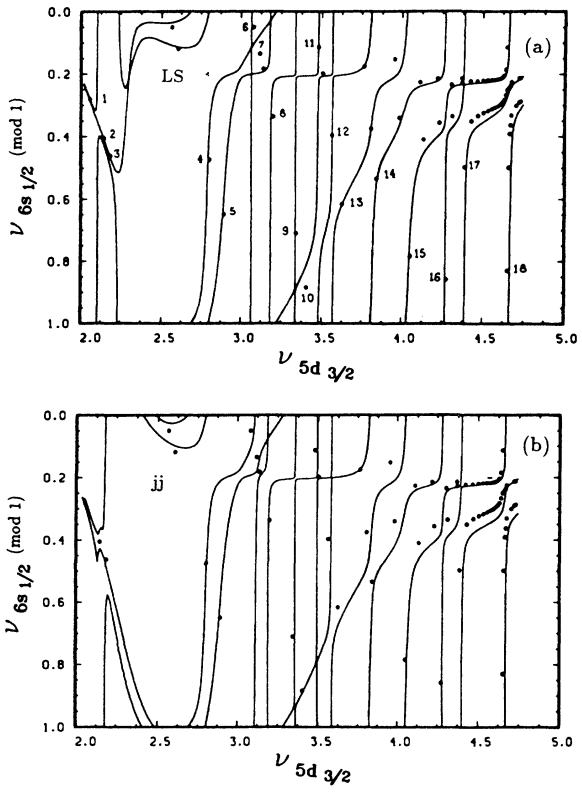

FIG. 9. Lu-Fano plot of the $J=2$ even-parity bound levels of Ba in the $-\nu_{6s}$ (mod 1) against the $\nu_{5d_{3/2}}$ plane. (a) ——, LS calculation; ●, experimental level positions [18,27,31,34]. Level assignments recommended by the present jj calculation are as follows: $5d^2\ ^3F_2$, $^1D_2$, $^3P_2$, (1,2,3); $5d7s\ ^3D_2$, $^1D_2$, (4,5); $6p^2\ ^3P_2$, $^1D_2$, (6,7); $5d6d\ ^3D_2$, $^3F_2$, (8,9); $6s7d\ ^1D_2$, (10); $5d6d\ ^1D_2$, $^3P_2$, (11,12); $6s8d\ ^1D_2$, (13); $5d8s\ ^3D_2$, $^1D_2$, (14,15); $5d7d\ ^3D_2$, $^3F_2$, $^1D_2$, (16,17,18). These classifications are discussed further in the text and in Table II. (b) ——, jj calculation.

We now turn to a comparison of the MQDT channel-mixing parameters obtained at the $6s$ threshold, either empirically or from R-matrix calculations. To better analyze the departures from the frame transformation, instead of the eigenvectors $U_{i\alpha}$ of the jj-coupled K matrix, we compare instead the eigenvectors $V_{\bar{\alpha}\alpha}$ of the matrix R^tKR, where R denotes the jj-LS geometric recoupling transformation. The $\bar{\alpha}$ channels correspond to pure LS-coupled channels. The α channels are the exact eigenchannels of the reaction matrix. If spin-orbit effects are negligible within the reaction volume, the matrix $V_{\bar{\alpha}\alpha}$ is expected to be block diagonal. The only MQDT parameters whose values are close in the three different treatments are the eigenquantum defects μ_α associated with

TABLE II. Positions of four experimental $J=2^e$ levels of Ba, showing the new classifications obtained in the present *jj*-coupled calculation.

Level number	Energy (cm^{-1})	Label Ref. [18]	Label Ref. [30]	*jj* result
6	35 344.42	$6p^2\,{}^1D_2$	$6s7d\,{}^1D_2$	$6p^2\,{}^3P_2$[a]
7	35 616.94	$6p^2\,{}^3P_2$		$6p^2\,{}^1D_2$[a]
10	37 434.95	$6s7d\,{}^1D_2$	$6s8d\,{}^1D_2$	$6s7d\,{}^1D_2$
13	38 556.18	$6s8d\,{}^1D_2$	$6p^2\,{}^1D_2$	$6s8d\,{}^1D_2$

[a]Levels 6 and 7 are so strongly mixed that these classifications should not be taken too seriously.

the $5dns$ and $5dnd$ channels and the $V_{\bar{\alpha}\alpha}$ matrix elements describing the mixing between the $6snd$ and $6pnp$ $^1D_2$ channels; the corresponding channel mixing, with a channel-mixing angle $\sim 0.2\pi$, clearly dominates the $J=2^e$ bound spectrum of Ba. Within the diagonal blocks corresponding to a given *LS* symmetry, the matrix elements deduced from the *jj*-coupled *R*-matrix calculation bear a close resemblance to those obtained by neglecting spin-orbit terms in the reaction volume. Both *R*-matrix calculations differ considerably from the matrices fitted to experiment. In particular, the mixing between perturbing channels, almost completely neglected in Ref. [30], is not negligible. The *R*-matrix calculation in *jj*-coupling shows strong departures from the *jj*-*LS* frame transformation, mainly within the three $6pnp$ channels and for other channels interacting with the $6pnp$ channels. Except for the $6snd$-$6pnp$ $^1D_2$ interaction, the empirical values introduced for several mixing angles are very different from those calculated with the *R*-matrix approach. In particular, the $6snd$ $^1D_2$ and $^3D_2$ eigenchannels are almost uncoupled (mixing angle ~ 0.02 rad) while the empirical value derived from hyperfine measurements was 0.42. Clearly, the neglect of the spin-orbit interaction for the $6p$ electron and the various other approximations involved in the empirical treatments affects the MQDT parameters considerably.

The preceding paragraph shows that quite different sets of MQDT parameters can give energy levels in good agreement. A good description of level positions is clearly necessary but not sufficient to demonstrate that a proper description of channel interactions has been achieved. Data on more sensitive observables are needed to probe the wave functions. This point has been largely documented in Ref. [4] for the even-parity $J=2$ spectrum of Ba. We have already mentioned that the new designations of levels 6 and 7 in Fig. 9 are supported by several experiments [33]. Now we consider another example in greater detail. It is known that hyperfine-structure measurements provide a very sensitive probe of the singlet-triplet mixing in high-lying $6snd$ levels. Figure 10 illustrates the evolution with n of the admixture coefficient β of the $6snd$ $^3D_2$ channel in the high-lying $5d7d$ and $6snd$ $^1D_2$ levels. The plus and cross symbols marked are derived from the hyperfine measurements of Eliel and Hogervorst [35], and those of Rinneberg and Neukammer [36], respectively. Note that β is an amplitude characterizing the singlet-triplet mixing, which is constrained to lie in the range $-1/\sqrt{2}\le\beta\le 1/\sqrt{2}$. The value $\beta=0$ is obtained only when S ($=0$ or 1) is a good quantum number, whereas the equal mixing of singlet and triplet states is obtained when β approaches one of the extrema just noted. For the explicit definition, see Refs. [35] and [36]. The dashed and solid curves are drawn through the theoretical *LS* and *jj* values, respectively. Compared to experiment, both theoretical curves are slightly shifted to the right, the predicted $5d7d$ $^1D_2$ levels being a little too high. However, it is evident that the experimental behavior is better reproduced by the *R*-matrix calculation in *jj* coupling than by the one carried out in *LS* coupling.

3. *The $J=0$ and 2 even-parity autoionizing spectrum of Ba*

The even-parity spectrum of Ba below the $5d_{5/2}$ threshold has been investigated using multistep laser spectroscopy [28,29,37–39] the $5dnl$ levels being excited from several $5d6p$ bound levels. For $J=0^e$, these investigations led to the observation of the two $5d_{3/2}nd_{3/2}$ and $5d_{5/2}nd_{5/2}$ $J=0$ Rydberg series up to large-n values and to the identification [38] of the $6p^2\,{}^1S_0$ level with a broad autoionizing resonance at 48 000 cm^{-1}. For $J=2^e$, the eight expected series $5dns$, $5dnd$, and $5dng$ have been observed [28,39]. The autoionization widths observed for

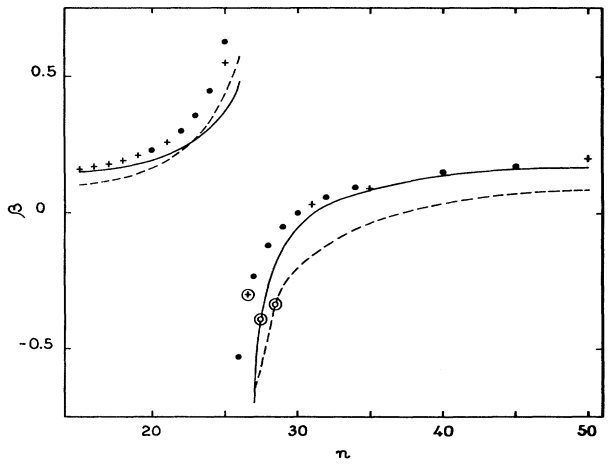

FIG. 10. Singlet-triplet β mixing coefficients for the high-lying $6snd$ $^1D_2$ and $5d7d$ $^1D_2$ levels of Ba. The *LS* results (— — —) and *jj* results (——) are compared with values deduced from hyperfine structure: ● [35], + [36]. The circled symbols correspond to the $5d7d$ $^1D_2$ level.

the $5dnd\ J=0$ and 2 resonances are much smaller than the separation between adjacent peaks. Thus, level identifications were obtained by analyzing the experimental data with empirical MQDT models ignoring the coupling with the $6s\epsilon l$ continua [28,37]. Moreover, for $J=2^e$, the $5dnd$-$5dng$ interaction was neglected. These studies, restricted to the positions of autoionizing resonances only, were completed by additional empirical MQDT studies which account for the interactions of autoionizing levels with the continua. A first theoretical description [38] dealt with the profiles of the $6p^2\,{}^1S_0$ level and of the nearby $5dnd\ J=0$ resonances. Later, the high-lying $5d_{3/2}nd_{3/2}$ levels were reinvestigated by Neukammer *et al.* [29] and dramatic deviations of the autoionization widths from the $\nu^{-3}_{5d_{3/2}}$ law (expected in the absence of channel interactions) have been observed, some levels being metastable against autoionization decay. This unusual suppression of the autoionization process for particular levels has been accurately described using MQDT [29,40]. Finally, Bente and Hogervorst [39] successfully used an MQDT parametrization to reproduce $J=2^e$ autoionizing features which they observed by photoionizing the $5d6p\ {}^1F_3$ bound level.

Most of the experimental photoionization measurements performed to date in the alkaline-earth atoms have been relative measurements which fail to provide an absolute scale to the cross section. Recently two absolute cross-section measurements were carried out for photoionization of the Ba $6s6p\ {}^1P^o_1$ state at energies near the $6s$ ionization threshold [41,42]. Two very recent calculations have obtained theoretical cross sections for comparison with these experiments, one a Wigner-Eisenbud R-matrix calculation by Bartschat and McLaughlin [43], and the other a jj-coupled R-matrix calculation by Greene and Theodosiou [44] using the same techniques described above. These two calculations are both in agreement that the measured cross sections of Kallenbach, Kock, and Zierer [41] are too large by a factor of approximately 5.5. On the other hand, the calculation of Ref. [44] suggests that the measured cross section of Burkhardt *et al.* [42] is correct in its absolute normalization to within a factor of 2.

Next we consider photoionization of excited barium $6s6p$ and $5d6p\ {}^1P_1$ levels into $J=0^e$ and $J=2^e$ final states. Channel-mixing parameters in the final $J=0^e$ and $J=2^e$ autoionizing energy range were obtained by performing variational calculations in either LS or jj coupling. The same l-dependent model potential $V(r)$ and two-electron basis set are used in both calculations (except that the spin-orbit interaction terms are, of course, omitted from the LS calculation). The wave functions of the initial state were obtained by diagonalizing, the two-electron Hamiltonian within the reaction volume. In the calculation done in LS coupling the starting level is assumed to be a pure $^1P_1$ level, this restriction being of course relaxed in the jj calculation. Also, the starting level is assumed to be isotropic in both calculations, ignoring the fact that it is typically aligned if prepared by laser excitation.

(a) The $J=0$ even-parity autoionizing spectrum of Ba. Figure 11 compares the LS and jj results obtained for the

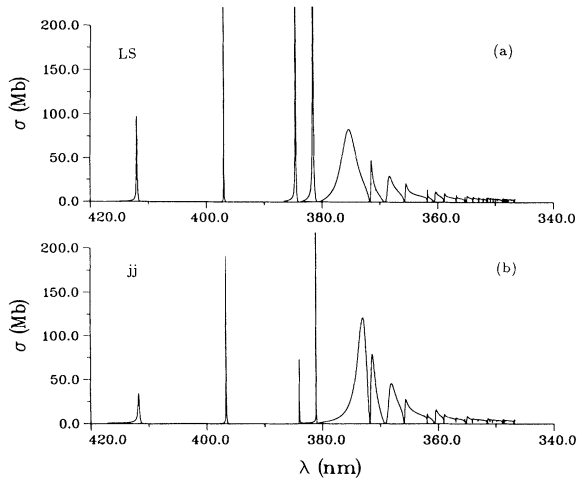

FIG. 11. Partial photoionization cross section for the $6s6p\ {}^1P_1 \rightarrow J=0^e$ symmetry of Ba in the wavelength region from 420 to 340 nm, below the $5d_{3/2}$ threshold. (a) LS results. (b) jj results.

$J=0^e$ partial photoionization cross section of the $6s6p\ {}^1P_1$ level of Ba, below the $5d_{3/2}$ threshold. As in the energy range below the $6s$ threshold, five channels are included in each calculation. Marked differences are visible in the 380–360-nm wavelength range where the $6p^2\,{}^1S_0$ level is expected to lie [38]. In the LS calculation this level is identified with the broad resonance around 375 nm, relatively well separated from the nearby $5d_{3/2}10d_{3/2}$ resonance in the right wing. In contrast, the jj spectrum shows a more complicated pattern of overlapping resonances. To achieve convergence in the $J=0^e$ R-matrix calculations it was found essential to include in the two-electron basis set strongly closed functions $nln'l$, involving large orbital momenta $l=3$ and 4. MQDT calculations performed with the K matrix deduced from the LS-coupled R-matrix calculation were performed using either experimental or theoretical threshold energies for the $6pnp$ channels; both calculations give almost identical results and thus the differences between curves 11(a) and 11(b) do not result from inaccuracies such as those which occur below the $6s$ threshold.

To better analyze the origin of the differences, we consider also the photoionization of the excited $5d6p\ {}^1P_1$ level, for which some observations are available. The LS and jj results obtained for the $5d6p\ {}^1P_1 \rightarrow J=0^e$ spectrum of Ba are compared in Fig. 12, in the same energy range as above. In addition, we indicate the positions of the resonance peaks observed by Camus *et al.* [28] and Aymar, Camus, and Hindy [38], the autoionizing levels being excited from the $5d6p\ {}^1P_1$ or $^3P_1$ level. Both curves 12(a) and 12(b), corresponding to LS or jj results respectively, correctly reproduce the positions of resonant peaks. Note that the differences between the calculated peak heights in curves 12(a) and 12(b) are not significant for the sharp resonances, curve 12(a) being obtained with a finer energy mesh than curve 12(b). However, near 45 000 cm^{-1}, the observed structures, i.e., the

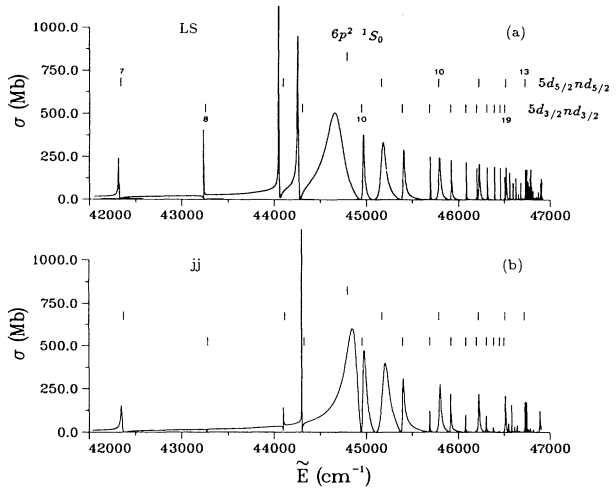

FIG. 12. Partial photoionization cross section for the $5d6p\ ^1P_1 \rightarrow J=0^e$ symmetry of Ba in the energy range 42 000 to 47 000 cm^{-1}, below the $5d_{3/2}$ thresold (the energies are relative to the ground state of Ba). (a) *LS* results; the vertical bars indicate the positions of observed autoionizing states [28,38]; some members of the $5d_{3/2}nd_{3/2}$ and $5d_{5/2}nd_{5/2}$ Rydberg series are labeled by their n value. (b) *jj* results.

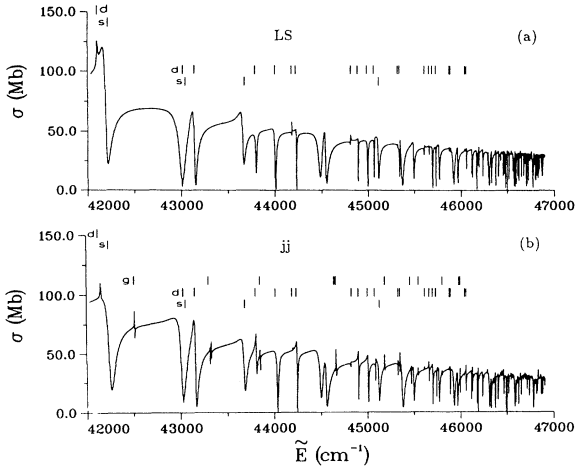

FIG. 13. Partial photoionization cross section for the $6s6p\ ^1P_1 \rightarrow J=2^e$ symmetry of Ba in the energy range 42 000 to 47 000 cm^{-1}, below the $5d_{3/2}$ threshold (the energies are relative to the ground state of Ba). (a) *LS* results (11-channel calculation); the vertical bars indicate the positions of autoionizing levels observed by Camus *et al.* [28]; the 5*dns* (*s*), 5*dnd* (*d*) and 5*dng* (*g*) are distinguished by the different ordinates used for the bars. (b) *jj* results (14-channel calculation).

broad and asymmetric resonance corresponding to the $6p^2\ ^1S_0$ level, and the nearby peak associated with the $5d_{3/2}10d_{3/2}$ level are better described by the *jj* calculation. The irregular variation of the autoionization widths along the $5d_{3/2}nd_{3/2}$ series, observed by Neukammer *et al.* [29], for $n \geq 14$, is already visible in Fig. 12 for smaller-n values. Because these observations have already been successfully interpreted we have not attempted to include enough energy points in our calculation to represent the spectrum just below the $5d_{3/2}$ threshold in greater detail.

The present calculations completely confirm the observations of Ref. [38] concerning the $6p^2$ autoionizing resonance. Note that the recent calculation of Bartschat and McLaughlin [43] fails to observe this level above the 6*s* threshold, in contrast to Ref. [44]. In addition, the small differences between curves (a) and (b) in Figs. 11 and 12 suggest a mild failure of the frame transformation for describing the $6p^2\ ^1S_0$ level. For this state, of course, the spin-orbit interaction must play the largest role among all members of the $6pnp\ ^1S_0$ Rydberg series.

(b) The $J=2$ even-parity autoionizing spectrum of Ba. Now we turn to the $J=2^e$ partial cross sections for photoionization of the $6s6p\ ^1P_1$ level of Ba, calculated below the $5d_{3/2}$ threshold. The 11 channels introduced in the R-matrix calculations done in *LS* coupling are identical to those used in calculating the bound spectra. In *jj* coupling, two different calculations were carried out, involving either 11 or 14 channels. The latter calculation treats the 5*dng* $J=2$ channels as "weakly closed," whereas the former calculation treats them as "strongly closed."

Figure 13 compares the 11-channel *LS* results with the 14-channel *jj* results. [The 11-channel *jj* calculation only differs from curve 13(b) by the absence of the sharp peaks associated with the 5*dng* resonances.] Curves 13(a) and 13(b) are in good agreement. In particular, the maxima of narrow peaks and minima are located at the same energies in both calculations. Especially in the lower-energy range, however, the shapes of the broad resonances show some noticeable differences. No experimental data are available for comparison except at particular energies [41,42] (see Fig. 3 of Ref. [44] for a comparison of theory and experiment).

To check the reliability of the calculations, positions of the resonances observed by Camus *et al.* [28] by photoionizing the $5d6p$ levels are marked by vertical bars. The predicted positions of the 5*dng* resonances [curve 13(b)] agree well with the observation. These sharp resonances are added to a more complex pattern of broad resonances separated by sharp windows. The detailed correspondence between these resonances and the observed 5*dns* and 5*dnd* levels is not obvious. To clarify the situation, we have calculated the $J=2^e$ partial photoionization cross section of the $5d6p\ ^1P_1$ level. The results of the 11-channel calculation done in *LS* coupling are compared on Fig. 14 with the same set of experimental level positions. Nearly every vertical bar can be associated without ambiguity to a calculated peak, the additional theoretical resonances being very weak. Moreover, we have verified that the previous assignments of levels are supported by our calculation. From Fig. 14, it is clear that the R-matrix description of the $J=2^e$ autoionizing resonance positions is accurate. The resonances displayed in Fig. 14 are relatively narrow, in agreement with the observations [28], but in apparent contradiction with Fig. 13.

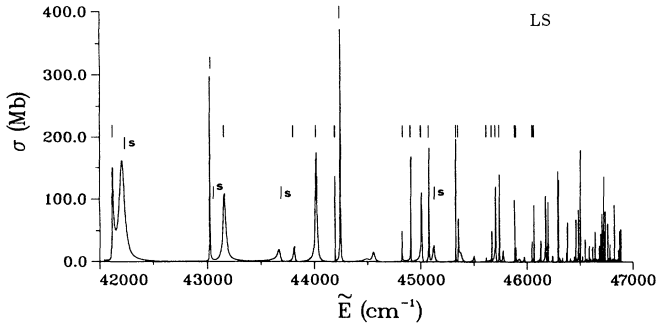

FIG. 14. Partial photoinozation cross section for the $5d6p\ ^1P_1 \rightarrow J=2^e$ symmetry of Ba, below the $5d_{3/2}$ threshold. The calculated *LS* results are shown as a solid curve, while vertical bars indicate the positions of auotionizing levels observed by Camus *et al.* [28]. All the bars indicate $5dnd$ resonances except those labeled by (*s*), which are associated with $5dns$ levels.

We now address the striking differences between Figs. 13 and 14. Since in both cases, the spectral density of the $J=2^e$ autoionizing states is the same, the differences must derive from differences in the mode of excitation of the resonances. In photoionization of the $5d6p$ level, the excitation of the $6s\epsilon l$ continua is negligible compared to that of the autoionizing Rydberg series $5dns,nd$ while the opposite holds for photoionization of the $6s6p$ level. For overlapping resonances, the distribution of oscillator strength is strongly affected by interference effects between autoionizing paths and direct photoionization paths, and as explained by Mies [45] the apparent widths of resonances depend on the excitation dipole matrix elements. Studying the case where two Rydberg series autoionize to the same continua, Mies [45] found two extreme cases when changing the Fano-profile indices of the series while other characteristics of the series remain unchanged. In these two cases, the oscillator strength is either collected in narrow intervals, giving sharp peaks like those visible in Fig. 14, or else it is spread out over a larger energy range while the cross section exhibits windows in narrow intervals, but with the narrow peaks and the sharp windows being located at the same places. Similar behavior is found here, as Fig. 13 shows that the positions of most of the dips between the broad resonances coincide with the peak positions in Fig. 14. These structures are much more complicated than in the case studied by Mies [45], however, owing to the large number of interloping Rydberg series. Note that similar broadening and narrowing effects also occur in Figs. 11 and 12, respectively. The small differences between the resonance profiles in curves (a) and (b) of Fig. 13 probably result from differences between calculated dipole matrix elements owing to the different selection rules which have been imposed in either *LS* or *jj* coupling. Experimental observation of the Ba $6s6p\ ^1P_1 \rightarrow J=2^e$ spectrum is desirable to probe the reliability of the calculations.

IV. DISCUSSION

This study demonstrates, along with the work discussed in Ref. [14], that an *R*-matrix calculation in *LS* coupling combined with a *jj*-*LS* MQDT frame transformation accurately describes channel interactions even in an atom as heavy as Ba. This conclusion is borne out by the good agreement between *LS*-coupling calculations and experiment, and also by the close agreement of the *LS*-coupled calculations with *jj*-coupled calculations, including spin-orbit terms in the short-range Hamiltonian explicitly. In atomic radium the agreement between these two methods of calculation deteriorates noticeably compared to barium, though more so in some spectral ranges than in others.

The complex and detailed spectral features and perturbations described in this paper give further evidence of the efficiency of the MQDT description at handling many interacting channels. Nevertheless, some of the difficulties encountered with the MQDT description should be pointed out. A first analytical complication occurs whenever the photoelectron energy in a channel i becomes less than $-1/2l_i^2$, at which point the "energy-normalized" Coulomb functions (f_i,g_i) become complex and therefore inconvenient. This complication is readily bypassed by matching to "analytic" Coulomb functions (f_i^0,g_i^0) in that particular channel [3(b)]. This modifies the linear MQDT equations in a standard manner (see, e.g., Eqs. (9)–(11) of Ref. [15]) and causes no further difficulties.

A more fundamental difficulty occurs whenever a channel is deeply enough closed for the exponential growth of its channel components to become "large" within the reaction zone $r \leq r_0$. Our experience has shown that several difficulties then arise. (i) The short-range MQDT parameters then acquire an appreciable r_0 dependence, although normally the calculated observables such as energy-level positions and photoabsorption intensities remain independent of r_0 to a good approximation. (ii) The same MQDT parameters begin to vary much more rapidly with energy in this range, in stark contrast to their smooth behavior closer to an ionization threshold. (iii) The use of experimental thresholds in such a strongly-closed channel can adversely affect the MQDT calculation of observables, sometimes producing artificial resonances and at other times causing a physical resonance or bound state to disappear altogether; as discussed in Sec. III, this last problem can be corrected by using theoretical ionization threshold energies in such channels for consistency. Examples of (i) and (ii) can be seen in some of the Lu-Fano plots of this paper. For instance, in Fig. 5 the theoretical *LS*-coupled and *jj*-coupled curves look complicated and extremely different at low energies, in contrast to the actual predicted bound levels, most of which agree reasonably well in the two calculations. These difficulties do not invalidate the use of MQDT in any way, but they require some caution and it will be desirable to eventually understand them better.

Another major conclusion of this paper and of Ref. [14] is that eigenchannel *R*-matrix methods are now capable of predicting the short-range parameters of

multichannel-quantum-defect theory for any atom having two valence electrons, to an accuracy which is spectroscopically useful. Reference [15] shows that this is true of the alkali-metal negative ions in addition to the neutral atoms treated in this paper. These computations are all comparatively modest, as the largest *jj*-coupled calculations have required only several hours of CPU time on a desktop computer workstation. To achieve spectroscopically useful results in the heavy alkaline-earth atoms like barium, the single most important element in the computational scheme is the use of a semiempirical potential $V(r)$ which generates one-electron levels (e.g., of Ba^+) in agreement with experiment. For the moment, such calculations have not been extended to the vicinity of thresholds much higher than the $6p$ thresholds of Ba^+. It should be possible to go as high in energy as the Ca calculations of Ref. [7(c)], without substantial modification of the present computer programs. However, the CPU time grows rapidly owing to the larger number of channels, and also owing to the larger value needed for the box radius r_0, which in turn demands more basis functions per channel to reach an equivalent level of convergence. Thus to go above the $8s$ threshold of Ba^+ would be somewhat more appropriate for high-speed supercomputers than for desktop workstations at their present level of technology.

A large number of previous MQDT analyses have been conducted semiempirically to interpret experimental data, especially in barium. Nearly all of these studies found that it is practically impossible to obtain enough experimental information to uniquely pin down the MQDT parameters in this fashion if the number of channels exceeds three of four. The success of small-scale calculations, like those of this paper, in calculating accurate short-range MQDT parameters should greatly help such analyses. Some discrepancies will always remain between theory and experiment, as in Fig. 9 for instance, and more generally whenever a perturber location is just slightly in error in the calculation. But even in such cases the calculated K matrix should serve as an excellent starting point for further semiempirical optimization.

It is familiar from many previous studies of atomic photoionization that observables relating to the *anisotropy* of the photoprocesses are more sensitive probes of wave-function accuracy than is the energy spectrum or the total photoionization cross section. A very recent study of Ba photoionization by Lange *et al.* [46] shows generally good agreement between measured and calculated photoelectron angular distribution asymmetry parameters β in several different channels. The calculations of Ref. [46] were conducted in *LS* coupling followed by a *jj-LS* frame transformation like the *LS* results of the present study. The origin of some remaining discrepancies between theoretical and experimental asymmetry parameters in Ref. [46] was further investigated by recalculating β using the present *jj*-coupled approach. While the *jj* and *LS* results are not completely identical, they both show comparable agreement with experiment, implying that the main limitations of these calculations do *not* stem from deficiencies of the *jj-LS* frame transformation, even in atomic barium.

Apparently these small deviations between theory and experiment in Ref. [46] derive instead from the model Hamiltonian used [Eq. (1)], which approximates the effect of the inner electrons by a semiempirical model potential which is (radially) local. Another possible source of error in some sensitive observables could be an incomplete convergence of the variational basis-set expansion, as this has not been exhaustively investigated. Most observables are relatively insensitive to the basis-set size, but there have been occasional indications (as in the unexpected importance of f and g states for describing the Ba $6p^2\,{}^1S_0$ resonance in Fig. 12) that a larger basis set might improve the convergence in some regions of the spectrum.

Despite the clear general success of the *jj-LS* frame transformation for barium, there are nevertheless a few specific instances where the fully *jj*-coupled calculations give improved agreement with the experimental spectrum. Examples visible from the present calculations include the low-lying $6p^2$ levels, specifically level number 3 in Fig. 8 which is the $6p^2\,{}^3P_0$ bound level, and the $6p^2\,{}^1S_0$ autoionizing level in Fig. 12. While the positions of these levels are accurately reproduced by the *jj*-coupled calculation, the *LS* calculation places the ${}^3P_0$ level too high and the ${}^1S_0$ level too low. This possibly indicates that the frame transformation underestimates the strength of the spin-orbit interaction for states in which the two electrons have a comparable degree of excitation. (This can be seen from the fact that this interaction tends to cause these two *LS*-coupled energy levels to repel each other.) Figure 10 also suggests that the singlet-triplet mixing is described somewhat more accurately by the *jj*-coupled calculation.

Finally, we point out again that the *jj*-coupled results are far more stable near the bottom end of each Rydberg series. In that energy range spurious results occasionally show up in the *LS*-coupled calculations using experimental threshold energies, as sometimes an unphysical bound (or quasibound) level may appear, or sometimes a physical bound level may disappear altogether. The origin of this instability is now well understood, relating to the exponential growth of strongly closed channel components. Use of the frame-transformation method in this energy range requires extra caution, and in some cases it is essential to use *theoretical* threshold energies for such channels [see item (iii) above], rather than experimental thresholds as are frequently used in MQDT.

A last question of some practical importance is whether the present calculations based entirely on a Schrödinger-level description of the valence electron dynamics can adequately describe relativistic effects. These are known to be important in heavy atoms such as barium and radium, yet all relativistic effects aside from the spin-orbit interaction are *apparently* neglected here. On this question we believe that, as discussed in Ref. [15], many relativistic effects on the two-electron spectrum such as the "relativistic mass correction" are indirectly incorporated through our use of a semiempirical one-electron model potential. In the course of adjusting the potential to reproduce experimental one-electron levels, we effectively guarantee that the phase of the outermost electron, e.g., in Ra^+, is correct at large distances $r \gtrsim 1$

a.u. This is the most important part of configuration space for determining the nature of valence electron-electron correlations, and the electron velocities are clearly small enough at these larger radii for the Schrödinger equation to suffice. Moreover, the dipole matrix elements used in calculating photoabsorption intensities are primarily sensitive to this region of configuration space beyond the inner shells. For these reasons we expect the present jj-coupled photoabsorption calculations, nonrelativistic except for the spin-orbit interaction, to be valid even for atomic radium. Less accurate results should be anticipated, on the other hand, for observables more sensitive to the wave function very close to the nucleus.

A better test of the accuracy of the present radium calculations is highly desirable, considering the sparse nature of available spectra. The Lu-Fano plots of Ra $J=1^e$ levels in Fig. 5 show generally good agreement between theory and experiment, as the calculated quantum defects μ_{7s} deviate by less than $\Delta\mu=0.05$ for all levels, except for two in Fig. 5. The exceptions include experimental level number 5 in Fig. 5, which apparently has no theoretical counterpart, and the theoretical level labeled T, having no experimentally observed counterpart. Judging from the accuracy of our calculations for Sr and Ba, and for most of the Ra levels, the most likely explanation of these major discrepancies is probably some type of experimental error or misclassification. Given our approximate treatment of relativistic effects, however, further theoretical and experimental effort is certainly needed before this conclusion can be confidently accepted.

ACKNOWLEDGMENTS

We thank M. Le Dourneuf, J. M. Launay, and P. G. Burke for their support and hospitality during a workshop in Meudon, France, where this work was initiated. We are grateful to U. Griesmann for providing us with cross-section photoionization data prior to publication. The work of one of us (C.H.G.) was supported in part by the National Science Foundation.

[1] C. H. Greene, Phys. Rev. A **28**, 2209 (1983); **32**, 1880 (1985); for the original iterative formulation, see also U. Fano and C. M. Lee, Phys. Rev. Lett. **31**, 1573 (1973).
[2] H. Le Rouzo and G. Raseev, Phys. Rev. A **29**, 1214 (1984).
[3] (a) M. J. Seaton, Rep. Prog. Phys. **46**, 97 (1983); (b) U. Fano and A. R. P. Rau, *Atomic Collisions and Spectra* (Academic, Orlando, 1986); (c) A. Giusti-Suzor and U. Fano, J. Phys. B **17**, 215 (1984); W. E. Cooke and C. L. Cromer, Phys. Rev. A **32**, 2725 (1985).
[4] M. Aymar, Phys. Rep. **110**, 163 (1984); M. Aymar, J. Opt. Soc. Am. B **1**, 239 (1984).
[5] C. H. Greene and Ch. Jungen, Adv. At. Mol. Phys. **21**, 51 (1985).
[6] (a) M. Aymar, J. Phys. B **20**, 6507 (1987); (b) M. Aymar, E. Luc-Koenig, and S. Watanabe, *ibid.* **20**, 4235 (1987); M. Aymar and J. M. Lecomte, *ibid.* **22**, 223 (1989).
[7] (a) C. H. Greene and L. Kim, Phys. Rev. A **36**, 2706 (1987); (b) L. Kim and C. H. Greene, *ibid* **36**, 4272 (1987); (c) **38**, 2361 (1988); (d) also V. Lange, U. Eichmann, and W. Sandner, J. Phys. B **22**, L361 (1989).
[8] (a) C. H. Greene, in *Fundamental Processes of Atomic Dynamics,* edited by J. Briggs, H. Kleinpoppen, and H. Lutz (Plenum, New York, 1988); (b) C. H. Greene and L. Kim, Phys. Rev. A **38**, 5953 (1988).
[9] See, e.g., T. N. Chang and Y. S. Kim, Phys. Rev. A **34**, 2609 (1986).
[10] I. I. Sobel'man, *An Introduction to the Theory of Atomic Spectra* (Pergamon, New York, 1972).
[11] C. M. Lee and K. T. Lu, Phys. Rev. A **8**, 1241 (1973); also K. T. Lu, J. Opt. Soc. Am. **64**, 706 (1974).
[12] J. A. Armstrong, J. J. Wynne, and P. Esherick, J. Opt. Soc. Am. **69**, 211 (1979).
[13] C. J. Dai, G. W. Schinn, and T. F. Gallagher, Phys. Rev. A **42**, 223 (1990); P. F. O'Mahony and C. H. Greene, *ibid.* **31**, 250 (1985); P. F. O'Mahony, *ibid.* **32**, 908 (1985).
[14] M. Aymar, J. Phys. B **23**, 2697 (1990).
[15] C. H. Greene, Phys. Rev. A **42**, 1405 (1990).
[16] U. Griesmann, B. Esser, and J. Hormes (unpublished).
[17] E. Rasmussen, Z. Phys. **87**, 607 (1934). For a relabeling of some levels see H. N. Russell, Phys. Rev. **46**, 989 (1934).
[18] C. E. Moore, *Atomic Energy Levels I–III,* Natl. Bur. Stand. (U.S.) Circ. No. 467 (U.S. GPO, Washington, DC, 1958).
[19] J. A. Armstrong, J. J. Wynne, and F. S. Tomkins, J. Phys. B **13**, L133 (1980); F. S. Tomkins and B. Ercoli, Appl. Opt. **6**, 1299 (1967).
[20] E. U. Condon and G. H. Shortley, *The Theory of Atomic Spectra* (Cambridge University Press, Cambridge, England, 1935).
[21] L. C. Biedenharn and J. D. Louck, *Angular Momentum in Quantum Physics* (Addision-Wesley, Reading, MA, 1981).
[22] R. D. Hudson, V. L. Carter, and P. A. Young, Phys. Rev. **180**, 77 (1969).
[23] F. Gounand, B. Carré, P. R. Fournier, P. d'Oliveira, and M. Aymar, J. Phys. B **24**, 1309 (1991).
[24] C. M. Brown and M. L. Ginter, J. Opt. Soc. Am. **68**, 817 (1978).
[25] L. Kim and C. H. Greene, J. Phys. B **22**, L175 (1989).
[26] J. J. Wynne and J. A. Armstrong, IBM J. Res. Dev. **23**, 490 (1979).
[27] M. Aymar, P. Camus, M. Dieulin, and C. Morillon, Phys. Rev. A **18**, 2173 (1978).
[28] P. Camus, M. Dieulin, and A. El Himdy, Phys. Rev. A **26**, 379 (1982); P. Camus, M. Dieulin, A. El Himdy, and M. Aymar, Phys. Scr. **27**, 125 (1983); M. Aymar, P. Camus, and A. El Himdy, *ibid.* **27**, 183 (1983).
[29] J. Neukammer, H. Rinneberg, G. Jönsson, W. E. Cooke, H. Hieronymus, A. König, K. Vietzke, and H. Springer Bolk, Phys. Rev. Lett. **55**, 1979 (1985).
[30] M. Aymar and O. Robaux, J. Phys. B **12**, 531 (1979); see also Ref. [4].
[31] J. Neukammer, G. Jönsson, A. König, K. Vietzke, H. Hieronymus, and H. Rinneberg, Phys. Rev. A **38**, 2804 (1988).
[32] J. Verges, unpublished result.
[33] J. E. Hunter III, J. S. Keller, and R. S. Berry, Phys. Rev.

A **33**, 3138 (1986); K. A. H. Leeuwen and W. Hogervorst, Z. Phys. A **316**, 149 (1984); W. H. King and M. Wilson, J. Phys. B **18**, 23 (1985).
[34] H. P. Palenius, Phys. Lett. A **56**, 451 (1976).
[35] E. R. Eliel and W. Hogervorst, J. Phys. B **16**, 1881 (1983).
[36] H. Rinneberg and J. Neukammer, Phys. Rev. A **27**, 1779 (1983); H. Rinneberg and J. Neukammer, J. Phys. B **15**, L825 (1982).
[37] J. J. Wynne and J. P. Hermann, Opt. Lett. **4**, 106 (1979).
[38] M. Aymar, P. Camus, and A. El Himdy, J. Phys. B **15**, L759 (1982).
[39] E. A. J. M Bente and W. Hogervorst, Z. Phys. D **14**, 119 (1989).
[40] M. Aymar, J. Phys. B **18**, L763 (1985).
[41] A. Kallenbach, M. Kock, and G. Zierer, Phys. Rev. A **38**, 2356 (1988).
[42] C. E. Burkhardt, J. L. Libbert, Jian Xu, J. J. Leventhal, and J. D. Kelley, Phys. Rev. A **38**, 5949 (1988).
[43] K. Bartschat and B. McLaughlin, J. Phys. B **23**, L439 (1990).
[44] C. H. Greene and C. E. Theodosiou, Phys. Rev. A **42**, 5773 (1990).
[45] F. Mies, Phys. Rev. **175**, 164 (1968).
[46] V. Lange, M. Aymar, U. Eichmann, and W. Sandner, J. Phys. B **24**, 91 (1991).